

Simulating Quantum Circuits by Model Counting

Jingyi Mei, Marcello Bonsangue and Alfons Laarman

Leiden University

Abstract. Quantum circuit compilation comprises many computationally hard reasoning tasks that nonetheless lie inside $\#\text{P}$ and its decision counterpart in PP . The classical simulation of general quantum circuits is a core example. We show for the first time that a strong simulation of universal quantum circuits can be efficiently tackled through weighted model counting by providing a linear encoding of Clifford+T circuits. To achieve this, we exploit the stabilizer formalism by Knill, Gottesmann, and Aaronson and the fact that stabilizer states form a basis for density operators. With an open-source simulator implementation, we demonstrate empirically that model counting often outperforms state-of-the-art simulation techniques based on the ZX calculus and decision diagrams. Our work paves the way to apply the existing array of powerful classical reasoning tools to realize efficient quantum circuit compilation; one of the obstacles on the road towards quantum supremacy.

Keywords: Quantum Computing · Quantum circuit simulation · Satisfiability · $\#\text{SAT}$ · Weighted Model Counting · Stabilizer Formalism.

1 Introduction

Classical simulation of quantum computing [66,4,73,17] serves as a crucial task in the verification [6,64,52,36], synthesis [13,58,3] and optimization [15,59] of quantum circuits. In addition, improved classical simulation methods aid the search for a quantum advantage [38,8].

Due to the inherent exponential size of the underlying representations of quantum states and operations, classical simulation of quantum circuits is a highly non-trivial task that comes in two flavors [51]: Weak simulators only sample the probability distribution over measurement outcomes, i.e, they implement the “bounded-error” BQP-complete problem that a quantum computer solves, whereas strong circuit simulators can compute the amplitude of any basis state, solving a $\#\text{P}$ -complete problem [27,39].

SAT-solvers [12,29] have shown great potential to solve many formal methods problems efficiently in practice. Likewise, for the (weighted) model counting problem, i.e, counting number (or weights) of satisfying assignments, many tools

can manage large sets of constraints within industrial applications [50,56], despite the $\#\text{P}$ -Completeness of the problem. Because strong quantum circuit simulation is $\#\text{P}$ -complete, weighted model counters are a natural fit that nonetheless has not yet been exploited. To do so, we provide the first encoding of the strong simulation problem of universal quantum circuits as a weighted model counting problem. Perhaps surprisingly, this encoding is linear in the number of gates or qubits, i.e., $\mathcal{O}(n+m)$ for m gates and n qubits.

One of the key properties of our encoding is that it does not use complex numbers to encode the probability amplitudes of quantum states—which would prohibit the use of all modern model counters—but merely requires negative weights. We achieve this by exploiting a generalization [72] of the Gottesman-Knill theorem [34], which in effect rewrites the density matrix of any quantum state in the stabilizer state basis [32], thereby obviating the need for complex numbers. It turns out many exact weighted model counters do support negative weights out of the box. Our encoding thus empowers them to reason directly about constructive interference, which is the cornerstone of all quantum algorithms.

Like many, our method builds on the Solovay–Kitaev theorem [26] that in particular shows that the Clifford+ T gate set is universal for quantum computing, meaning that this gate set can efficiently approximate any unitary operator. Since our encoding also supports arbitrary rotation gates (phase shift P , R_x , R_y and R_z), and since these rotations are non-Clifford gates, it can also support other universal gate sets like Clifford+ R_x or Clifford+ P , which allows for easier approximations. One important example is Quantum Fourier Transformation (QFT), which can be simulated with $\mathcal{O}(n)$ rotation gates while needs at least $\mathcal{O}(n \log(n))$ T gates to approximate [47]. Moreover, since the hardness of exact reasoning about quantum circuits depends on the gate set (the classes EQP and NQP are parameterized by the gate set as it defines the realizable unitaries), this flexibility greatly increases the strength of our strong simulation approach.

We implement our encoding in an open source tool QCMC, which uses the weighted model-counting tool GPMC [35]. We demonstrate the scalability and feasibility of the proposed encoding through experimental evaluations based on three classes of benchmarks: random Clifford+ T circuits mimicking quantum chemistry applications [71] and oracles, and quantum algorithms from MQT bench [54]. We compare the results of our method against state-of-the-art circuit simulation tools QuiZX [40] and Quasimodo [60], respectively based on the ZX-calculus [24] and CFLOBDD [61]. QCMC simulates important quantum algorithms like QAOA, W-state and VQE, etc, which are not supported by QuiZX. Additionally, QCMC outperforms Quasimodo on almost all random circuits and uses orders of magnitudes less memory than Quasimodo on all benchmarks.

In sum, this paper makes the following contributions.

- a generalized stabilizer formalism formulated in terms of stabilizer groups, which forms a basis for our encoding;

- the first encoding for circuits in various universal quantum gate sets as a weighted model counting problem, which is also linear in size;
- an implementation based on the weighted model counting tool GPMC;
- new benchmarks for the WMC competition [1], and insights on improving model counters and samplers for applications in quantum computing.

2 Preliminaries

2.1 Quantum Computing

Similar to bits in classical computing, a quantum computer operates on quantum bits, or short as *qubits*. A bit is either 0 or 1, while a qubit has states $|0\rangle$ or $|1\rangle$. Here ‘ $|\cdot\rangle$ ’ is the *Dirac notation*, standard in quantum computing, standing for a unit column vector, i.e., $|0\rangle = [1, 0]^T$ and $|1\rangle = [0, 1]^T$, while $\langle\psi|$ denotes the complex conjugate and transpose of $|\psi\rangle$, that is a row vector: $\langle\psi| = |\psi\rangle^\dagger$.

Let \mathcal{H} be a Hilbert space. A n -qubit quantum state is a 2^n -dimension unit column vector in \mathcal{H} . In the case of $n = 1$, a pure state $|\psi\rangle$ is written as $|\psi\rangle = \alpha|0\rangle + \beta|1\rangle$, where α and β are complex numbers in \mathbb{C} satisfying $|\alpha|^2 + |\beta|^2 = 1$. Sometimes we represent a pure quantum state $|\psi\rangle$ by the density operator obtained as the product $|\psi\rangle\langle\psi|$ of the state with itself. For the rest of the paper, we fix n to be the number of the qubits.

Operations on quantum states are given by *quantum gates*. For an n -qubit quantum system, a (global) quantum gate is a function $\mathbf{G} : \mathcal{H} \rightarrow \mathcal{H}$, which can be described by $2^n \times 2^n$ *unitary matrix* U , i.e., with the property that $UU^\dagger = U^\dagger U = I$. A quantum gate is *local* when it works on a subspace of quantum system, which can be extended to a *global quantum gate* by apply identity operators on unchanged qubits, i.e. a local quantum gate U on qubit i can be represented as a global quantum gate $U_i = \underbrace{I \otimes \dots \otimes I}_i \otimes U \otimes \underbrace{I \otimes \dots \otimes I}_{n-i-1}$. Examples of quantum gates are the following 2×2 *Pauli matrices* (or *Pauli gates*):

$$\sigma[00] \equiv I \equiv \begin{bmatrix} 1 & 0 \\ 0 & 1 \end{bmatrix}, \sigma[01] \equiv Z \equiv \begin{bmatrix} 1 & 0 \\ 0 & -1 \end{bmatrix}, \sigma[10] \equiv X \equiv \begin{bmatrix} 0 & 1 \\ 1 & 0 \end{bmatrix}, \sigma[11] \equiv Y \equiv \begin{bmatrix} 0 & -i \\ i & 0 \end{bmatrix}.$$

Pauli matrices form a basis for 2×2 Hermitian matrix space. Let PAULI_n be the set of the tensor product of n Pauli operators (a ‘‘Pauli string’’). Any density operator in an n -qubit system can be written as $\sum_i \alpha_i P_i$ where $P_i \in \text{PAULI}_n$ and α_i are real numbers [32]. The so-called Pauli group is generated by multiplication of the local Pauli operators X, Z as follows: $\mathcal{P}_n = \langle X_0, Z_0, \dots, X_{n-1}, Z_{n-1} \rangle$. Structurally, the Pauli group can now be written as $\mathcal{P}_n = \{k \cdot P \mid P \in \text{PAULI}_n, k \in \{\pm 1, \pm i\}\}$. For instance, we have $-X \otimes Y \otimes Z \in \mathcal{P}_3$.

The evolution of a quantum system can be modeled by a quantum circuit. Let $[m]$ be $\{0, \dots, m-1\}$. A quantum circuit is given by a sequence of quantum gates:

$C \equiv \mathbf{G}^0 \dots \mathbf{G}^{m-1}$, where $\mathbf{G}^t \in \mathcal{H}$ is a global quantum gate at time step $t \in [m]$. Let U^t be the unitary matrix for \mathbf{G}^t . Then C is represented by the unitary matrix $U = U^{m-1} \dots U^0$.

An important class of quantum circuits is the so-called Clifford class or group, as they can describe interesting quantum mechanical phenomena such as entanglement, teleportation, and superdense encoding. More importantly, they are widely used in quantum error-correcting codes [18,62] and measurement-based quantum computation [55]. The Clifford group is the set of unitary operators that map the Pauli group to itself through conjugation, i.e. all the $2^n \times 2^n$ unitary matrices U such that $UPU^\dagger \in \mathcal{P}_n$ for all $P \in \mathcal{P}_n$. It is generated by the local Hadamard (H) and phase (S) gates, and the two-qubit control-not gate (CX , $CNOT$):

$$H = \frac{1}{\sqrt{2}} \begin{bmatrix} 1 & 1 \\ 1 & -1 \end{bmatrix}, \quad S = \begin{bmatrix} 1 & 0 \\ 0 & i \end{bmatrix}, \quad \text{and } CX = \begin{bmatrix} 1 & 0 & 0 & 0 \\ 0 & 1 & 0 & 0 \\ 0 & 0 & 0 & 1 \\ 0 & 0 & 1 & 0 \end{bmatrix}.$$

Recall that U_j performs U on j -th qubit. Similarly, we denote by CX_{ij} the unitary operator taking the i -th qubit as the control qubit and j -qubit as the target to execute a controlled-not gate. Clifford circuits are circuits only containing gates from the Clifford group.

A (projective) measurement is given by a set of *projectors* $\{\mathbb{P}_0, \dots, \mathbb{P}_{k-1}\}$ —one for each measurement outcome $[k]$ —satisfying $\sum_{j \in [k]} \mathbb{P}_j = I$. A linear operator \mathbb{P} is a projector if and only if $\mathbb{P}\mathbb{P} = \mathbb{P}$. For example, given a 3-qubit system, measuring the first 2 qubits under computational basis is given by projective measurement $\{ |0\rangle\langle 0| \otimes |0\rangle\langle 0| \otimes I, |1\rangle\langle 1| \otimes |0\rangle\langle 0| \otimes I, |0\rangle\langle 0| \otimes |1\rangle\langle 1| \otimes I, |1\rangle\langle 1| \otimes |1\rangle\langle 1| \otimes I \}$.

Weak simulation is the problem of sampling the measurements outcomes according to the probability distribution induced by the semantics of the circuit. In this work, we focus on strong simulation as defined in Definition 1. Here we assume, without loss of generality, that a circuit is initialized to the all-zero state: $|0\rangle^{\otimes n}$.

Definition 1 (The strong simulation simulation). *Given an n -qubit quantum circuit C and a measurement $M = \{\mathbb{P}_0, \dots, \mathbb{P}_{k-1}\}$, a strong simulation of circuit C computes the probability of getting any outcome $l \in [k]$, that is, the value $\langle 0 |^{\otimes n} C^\dagger \mathbb{P}_l C | 0 \rangle^{\otimes n}$, up to a number of desired bits of precision.*

The Gottesman-Knill theorem [34] shows that Clifford circuits can be strongly simulated by classical algorithms in polynomial time and space.

2.2 Stabilizer Groups

The stabilizer formalism [34] is a subset of quantum computing that can be effectively simulated on a classical computer. A state $|\varphi\rangle$ is said to be *stabilized* by a quantum unitary operator U if and only if it is a $+1$ eigenvector of U , i.e., $U|\varphi\rangle = |\varphi\rangle$. For example, we say $|0\rangle$ is *stabilized* by Z as $Z|0\rangle = |0\rangle$. Similarly,

$|+\rangle = \frac{1}{\sqrt{2}}|0\rangle + \frac{1}{\sqrt{2}}|1\rangle$ is stabilized by X , and all states are stabilized by I . The *stabilizer states* form a strict subset of all quantum states which can be uniquely described by maximal commutative subgroups of the Pauli group \mathcal{P}_n , which is called *stabilizer group*. The elements of the stabilizer group are called *stabilizers*. Recall that the Clifford group is formed by unitary operators mapping the Pauli group to itself. This leads to the fact that stabilizer states are closed under operators from the Clifford group.

Given an n -qubit stabilizer state $|\psi\rangle$, let $\mathcal{S}_{|\psi\rangle}$ be the stabilizer group of $|\psi\rangle$. While the elements of a Pauli group \mathcal{P}_n either commute or anticommute, a stabilizer group \mathcal{S} must be abelian, because if $P_1, P_2 \in \mathcal{S}_{|\varphi\rangle}$ anticommute, i.e. $P_1 P_2 = -P_2 P_1$, there would be a contradiction: $|\varphi\rangle = P_1 P_2 |\varphi\rangle = -P_2 P_1 |\varphi\rangle = -|\varphi\rangle$. In particular, $-I^{\otimes n}$ can never be a stabilizer. In fact, a subgroup \mathcal{S} of \mathcal{P}_n is a stabilizer group for an n -qubit quantum state if and only if it is an abelian group without $-I^{\otimes n}$. Therefore, for any Pauli string $\mathbf{P} \in \text{PAULI}_n$, if $k\mathbf{P} \in \mathcal{S}$, we have $k = \pm 1$, since $\forall k\mathbf{P} \in \mathcal{S} : (k\mathbf{P})|\varphi\rangle = (k\mathbf{P})^2|\varphi\rangle = k^2 I|\varphi\rangle = k^2|\varphi\rangle \Rightarrow k = \pm 1$. For clarity, we will use the symbols P for Pauli strings with weight and use symbol \mathbf{P} for Pauli strings without weight, i.e. $\mathbf{P} \in \text{PAULI}$.

As every subgroup of a free group is free, any stabilizer group \mathcal{S} can be specified by a set of generators \mathcal{G} so that every element in \mathcal{S} can be obtained through matrix multiplication on \mathcal{G} , denoted as $\langle \mathcal{G} \rangle = \mathcal{S}$. The set of generators \mathcal{G} needs not to be unique and has order $|\mathcal{G}| = n$, where n represents the number of qubits, and the corresponding stabilizer group \mathcal{S} has order $2^{|\mathcal{G}|}$.

Example 1. The Bell state $|\Phi_{00}\rangle = \frac{1}{\sqrt{2}}(|00\rangle + |11\rangle)$ can be represented by the following stabilizer generators written in square form:

$$\frac{1}{\sqrt{2}}(|00\rangle + |11\rangle) \equiv \left\langle \begin{array}{c} X \otimes X \\ Z \otimes Z \end{array} \right\rangle \equiv \left\langle \begin{array}{c} X \otimes X \\ -Y \otimes Y \end{array} \right\rangle. \quad \square$$

We can relate the (generators of the) stabilizer group directly to the stabilizer state $|\psi\rangle$, as the density operator of the stabilizer state can be written in a basis of Pauli matrices as follows [65]:

$$|\psi\rangle\langle\psi| = \prod_{G \in \mathcal{G}_{|\psi\rangle}} \frac{I+G}{2} = \frac{1}{2^n} \sum_{P \in \mathcal{S}_{|\psi\rangle}} P. \quad (1)$$

If a Clifford gate U is applied to the above state, i.e. $U|\psi\rangle$, and let $P \in \mathcal{S}_{|\psi\rangle}$, the corresponding stabilizers of $U|\psi\rangle$ can be obtained by UPU^\dagger since $UPU^\dagger U|\psi\rangle = U|\psi\rangle$. Thus we have $\mathcal{S}_{U|\psi\rangle} = \{UPU^\dagger \mid P \in \mathcal{S}_{|\psi\rangle}\}$ and the density operator of the resulting state will be obtained by conjugating U on $|\psi\rangle\langle\psi|$, i.e. $U|\psi\rangle\langle\psi|U^\dagger = \frac{1}{2^n} \sum_{P \in \mathcal{S}_{|\psi\rangle}} UPU^\dagger$. To be specific, consider performing a Clifford gate U_j , denoting a single qubit gate U applied to j -th qubit as given in previous section, to a stabilizer $P = P_1 \otimes \dots \otimes P_n$ where $P \in \mathcal{S}_{|\psi\rangle}$. We have $U_j P U_j^\dagger = P_1 \otimes \dots \otimes U P U^\dagger \otimes \dots \otimes P_n$. Since U is a Clifford gate, $U P U^\dagger \in \mathcal{P}_n$. Thus only the sign k and the

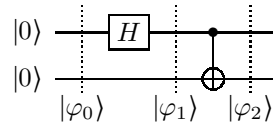
Table 1: Lookup table for the action of conjugating Pauli gates by T gates. The subscripts “c” and “t” stand for “control” and “target”. Adapted from [31].

Gate	In	Out	Gate	In	Out
H	X	Z	CX	$I_c \otimes X_t$	$I_c \otimes X_t$
	Y	$-Y$		$X_c \otimes I_t$	$X_c \otimes X_t$
	Z	X		$I_c \otimes Y_t$	$Z_c \otimes Y_t$
S	X	Y		$Y_c \otimes I_t$	$Y_c \otimes X_t$
	Y	$-X$		$I_c \otimes Z_t$	$Z_c \otimes Z_t$
	Z	Z		$Z_c \otimes I_t$	$Z_c \otimes I_t$

j -th entry need to be updated, which can be done in constant time following the rules in Table 1 for H and S . Applying a two-qubit gate CX_{ij} is similar to updating the sign and Pauli matrices in i -th and j -th position (see Table 1), which also takes constant time. Overall, updating all generators after performing one Clifford gate can be done in $O(n)$ time.

Although stabilizer states are a subset of quantum states, the space of density matrices for n -qubit states has a basis consisting of density matrices of n -qubit stabilizer states [32], which makes it possible to extend the stabilizer formalism to a general quantum state.

Example 2. The Bell state $|\Phi_{00}\rangle = \frac{1}{\sqrt{2}}(|00\rangle + |11\rangle)$ is a stabilizer state, as it can be obtained by the following circuit, which evaluates to $CX_{01} \cdot H_0 \cdot |00\rangle = |\Phi_{00}\rangle$:



We can simulate the above circuit with the stabilizer formalism. The stabilizer generator set for each time step can be obtained using the rules shown in Table 1:

$$\begin{pmatrix} Z \otimes I \\ I \otimes Z \end{pmatrix} \xrightarrow{H_0} \begin{pmatrix} HZH^\dagger \otimes I \\ H I H^\dagger \otimes Z \end{pmatrix} = \begin{pmatrix} X \otimes I \\ I \otimes Z \end{pmatrix} \xrightarrow{CX_{0,1}} \begin{pmatrix} CX(X \otimes I)CX^\dagger \\ CX(I \otimes Z)CX^\dagger \end{pmatrix} = \begin{pmatrix} X \otimes X \\ Z \otimes Z \end{pmatrix}. \quad \square$$

According to the Gottesmann-Knill Theorem, a quantum circuit can be effectively simulated when it starts from a stabilizer state and contains exclusively Clifford gates [34]. Because of the small number of generators needed, stabilizer groups can be used for an effective classical simulation of quantum states. In a 2^n -dimensional Hilbert space, instead of describing a quantum state by a 2^n complex-valued vector, one can use its stabilizer generator set to indicate the quantum state.

It's important to note that Clifford gates don't constitute a universal set of quantum gates. Certain unitary operators, like the T gate represented by $T = |0\rangle\langle 0| + e^{i\pi/4}|1\rangle\langle 1|$, fall outside this set. However, by augmenting the set of Clifford gates with the T gate, it becomes possible to approximate any unitary operator with arbitrary accuracy, as shown in [41,14].

2.3 Weighted Model Counting

Weighted model counters can solve probabilistic reasoning problems like Bayesian inference [20]. In these “classical” settings, the weights in the encoding of e.g. a Bayesian network represent positive probabilities. The quantum setting that we study here is well-known for its complex probabilities, called amplitudes. However, by expressing (pure) quantum states as their density matrices, and rewriting those in the stabilizer basis [32], we obviate the need for complex numbers, as shown in the next section. It turns out that existing weighted model counting tools, like GPMC [35], already support negative weights (see Section 4).

Let \mathbb{B} be the Boolean set $\{0, 1\}$. A propositional formula $C: \mathbb{B}^V \rightarrow \mathbb{B}$ over a finite set of Boolean variables V is *satisfiable* if there is an assignment $\alpha \in \mathbb{B}^V$ such that $C(\alpha) = 1$. We define the set of all satisfiable assignments of a propositional formula C as $SAT(C) := \{\alpha \mid \alpha(C) = 1\}$. We write an assignment α as a *cube* (a conjunction of literals, i.e. positive or negative variables), e.g., $a \wedge b$, or shorter ab .

A weight function $W: \{\bar{v}, v \mid v \in V\} \rightarrow \mathbb{R}$ assigns to the positive literal v (i.e., $v = 1$) and the negative literal \bar{v} (i.e., $v = 0$) a real-valued weight. We say variable v is *unbiased* iff $W(v) = W(\bar{v}) = 1$. Given an assignment $\alpha \in \mathbb{B}^V$, let $W(\alpha(v)) = W(v = \alpha(v))$ for $v \in V$.

For a propositional formula C over variables in V and weight function W , we define *weighted model counting* as follows.

$$MC_W(C) \triangleq \sum_{\alpha \in \mathbb{B}^V} C(\alpha) \cdot W(\alpha), \text{ where } W(\alpha) = \prod_{v \in V} W(\alpha(v)).$$

Example 3. Given a propositional formula $C = v_1 v_2 \vee \bar{v}_1 v_2 \vee v_3$ over $V = \{v_1, v_2, v_3\}$, there are two satisfying assignments: $\alpha_1 = v_1 v_2 v_3$ and $\alpha_2 = \bar{v}_1 v_2 v_3$. We define the weight function W as $W(v_1) = -\frac{1}{2}$, $W(\bar{v}_1) = \frac{1}{3}$ and $W(v_2) = \frac{1}{4}$, $W(\bar{v}_2) = \frac{3}{4}$, while v_3 remains unbiased. The weight of C can be computed as $MC_W(C) = -\frac{1}{2} \times \frac{1}{4} \times 1 + \frac{1}{3} \times \frac{1}{4} \times 1 = -\frac{1}{24}$. \square

3 Encoding Quantum Circuits as Weighted CNF

3.1 Generalized stabilizer formalism

Clifford circuits together with T gates generate states beyond stabilizer states, enabling universal quantum computation. As is shown in Table 1, Clifford gates map the set of Pauli matrices to itself, keeping stabilizers within the Pauli group. In contrast, T gates can transform a Pauli matrix into a linear combination of Pauli matrices. To be specific, Table 2 gives the action of T gates on different Pauli gates. Given a Pauli string, after performing Clifford+ T gates, we will get a summation of weighted Pauli strings, e.g., $T_1 \cdot (X \otimes X) \cdot T_1^\dagger = \frac{1}{\sqrt{2}}(X \otimes X + Y \otimes X)$.

This leads to the definition of *generalized stabilizer state* extended from standard stabilizer formalism.

Definition 2. *In a n -qubit quantum system, a generalized stabilizer state $|\psi\rangle$ is the simultaneous eigenvector, with eigenvalue 1, of a group containing 2^n commuting unitary operators S . The set of S is a generalized stabilizer group.*

The above definition is adapted from [72] by defining a generalized stabilizer state using a generalized stabilizer group instead of generalized stabilizer generators. In this way, we can easily get the corresponding stabilizer state by a weighted summation of its stabilizers to avoid multiplications between Pauli strings (the middle part of Eq. 1). The following proposition is also adapted from [72], where they demonstrate that any pure state can be uniquely described by a set of stabilizers. We additionally show that there exists a set of stabilizers, forming a group, which uniquely describes any pure state.

Proposition 1. *For any pure state $|\varphi\rangle$ in a n -qubit quantum system, there exists a generalized stabilizer group $\mathcal{S}_{|\varphi\rangle}$ such that $|\varphi\rangle\langle\varphi| = \frac{1}{2^n} \cdot \sum_{P \in \mathcal{S}_{|\varphi\rangle}} P$.*

Proof. Given a pure state $|\varphi\rangle$, we have $|\varphi\rangle = U|0\rangle^{\otimes n}$, where U is a unitary operator. Let $\mathcal{S}_{|\varphi\rangle} = \{USU^\dagger \mid S \in \mathcal{S}_{|0\rangle^{\otimes n}}\}$, which is an isomorphic group to $\mathcal{S}_{|0\rangle}$ since U is unitary. For any $S \in \mathcal{S}_{|\varphi\rangle}$, we have $S' \in \mathcal{S}_{|0\rangle^{\otimes n}}$ satisfying $S = US'U^\dagger$ and $S|\varphi\rangle = US'U^\dagger U|0\rangle^{\otimes n} = US'|0\rangle^{\otimes n} = U|0\rangle^{\otimes n} = |\varphi\rangle$. Hence $\mathcal{S}_{|\varphi\rangle}$ is the generalized stabilizer group of state $|\varphi\rangle$. Furthermore, we have $|\varphi\rangle\langle\varphi| = U|0\rangle\langle 0|U^\dagger = U(\frac{1}{2^n} \sum_{S' \in \mathcal{S}_{|0\rangle^{\otimes n}}} S')U^\dagger = \frac{1}{2^n} \sum_{S' \in \mathcal{S}_{|0\rangle^{\otimes n}}} US'U^\dagger = \frac{1}{2^n} \cdot \sum_{S \in \mathcal{S}_{|\varphi\rangle}} S$. In fact, since any generalized stabilizer $S \in \mathcal{S}_{|\varphi\rangle}$ is a Hermitian matrix, as $S = US'U^\dagger = US'^\dagger U = S^\dagger$ with $S' \in \mathcal{S}_{|0\rangle}$, it can be written as $S = \sum_i \alpha_i P_i$ where $P_i \in \text{PAULI}_n$ and α_i are real numbers satisfying $\sum_i \alpha_i^2 = 1$. Thus a generalized stabilizer is always a linear combination of stabilizers. \square

For a n -qubit quantum space, let $GStab$ be the set of generalized stabilizer states, which is also the set of all pure states. Let \mathcal{Q} be the set of quantum states generated from a Clifford+ T circuit starting from the all-zero state, i.e. $\mathcal{Q} = \{U_{m-1} \dots U_0 |0\rangle^{\otimes n} \mid U_i \in \{H, S, CX, T\}\}$. We have $Stab \subset \mathcal{Q} \subset GStab$ and

Table 2: Lookup table for the action of conjugating Pauli gates by T gates.

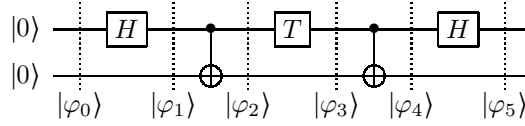
Gate	In	Out	Short
T	X	$\frac{1}{\sqrt{2}}(X + Y)$	$\triangleq X'$
	Y	$\frac{1}{\sqrt{2}}(Y - X)$	$\triangleq Y'$
	Z	Z	

any pure state in $GStab$ can be approximated by some state in \mathcal{Q} with arbitrary accuracy [26]. For any $|\varphi\rangle \in Stab$, we have $\mathcal{S}_{|\varphi\rangle} = \{P \mid P \in \text{PAULI}_n\}$. For any $|\psi\rangle \in GStab$, we have $\mathcal{S}_{|\psi\rangle} = \{\sum_i \alpha_i P_i \mid P_i \in \text{PAULI}_n, \alpha_i \in \mathbb{R}\}$. E.g., when applying Clifford+ T gates on $|\varphi\rangle$, we get generalized stabilizer state $|\psi\rangle$ with $\mathcal{S}_{|\psi\rangle} = \{\sum_i \pm(\frac{1}{\sqrt{2}})^{k_i} P_i \mid P_i \in \text{PAULI}_n, k_i \in \mathbb{N}^+\}$ (by updating $\mathcal{S}_{|\varphi\rangle}$ based on Table 1 and Table 2). Combining with Proposition 1, we may flatten summations:

$$|\psi\rangle\langle\psi| = \frac{1}{2^n} \sum_{S \in \mathcal{S}_{|\psi\rangle}} \sum_i \pm(\frac{1}{\sqrt{2}})^{k_i} P_i = \sum \pm(\frac{1}{\sqrt{2}})^{k_i} P_i. \quad (2)$$

Hence the density operator is determined by a summation of weighted Pauli strings and there is no need to distinguish which of the 2^n generalized stabilizers a Pauli string belongs to. We exploit this in our encoding and Example 4.

Example 4. Reconsider the circuit in Example 2 and add T , CX and H gate:



Continuing from Example 2, we obtain the following generalized generators.

$$\underbrace{\begin{pmatrix} X \otimes X \\ Z \otimes Z \end{pmatrix}}_{|\varphi_2\rangle} \xrightarrow{T_0} \underbrace{\begin{pmatrix} X' \otimes X \\ Z \otimes Z \end{pmatrix}}_{|\varphi_3\rangle} \xrightarrow{CX_{0,1}} \underbrace{\begin{pmatrix} X' \otimes I \\ I \otimes Z \end{pmatrix}}_{|\varphi_4\rangle} \xrightarrow{H_0} \underbrace{\begin{pmatrix} Z' \otimes I \\ I \otimes Z \end{pmatrix}}_{|\varphi_5\rangle},$$

where $X' = \frac{1}{\sqrt{2}}(X + Y)$ and $Z' = \frac{1}{\sqrt{2}}(Z - Y)$.

In our encoding, as in the above definition of generalized stabilizer states, we let satisfying assignments represent not just the generator set, but the entire stabilizer groups. These groups are: $\mathcal{S}_{|\varphi_2\rangle} = \{X \otimes X, Z \otimes Z, -Y \otimes Y, I \otimes I\}$, $\mathcal{S}_{|\varphi_3\rangle} = \{X' \otimes X, Z \otimes Z, -Y' \otimes Y, I \otimes I\}$, $\mathcal{S}_{|\varphi_4\rangle} = \{X' \otimes I, I \otimes Z, X' \otimes Z, I \otimes I\}$ and $\mathcal{S}_{|\varphi_5\rangle} = \{Z' \otimes I, I \otimes Z, Z' \otimes Z, I \otimes I\}$, where $Y' = \frac{1}{\sqrt{2}}(Y - X)$.

Finally, according to Eq. 2, we may equally expand e.g. $\mathcal{S}_{|\varphi_5\rangle}$ to:

$$\mathcal{S}'_{|\varphi_5\rangle} = \left\{ \frac{1}{\sqrt{2}}Z \otimes I, -\frac{1}{\sqrt{2}}Y \otimes I, I \otimes Z, \frac{1}{\sqrt{2}}Z \otimes Z, -\frac{1}{\sqrt{2}}Y \otimes Z, I \otimes I \right\}. \quad \square$$

3.2 Encoding Clifford+T circuits

Since generalized stabilizer states can be determined by a sum of weighted Pauli strings as shown in Eq. 2, we encode a state by Boolean constraints whose satisfying assignments represent those weighted Pauli strings. The idea is to encode the sign, the Pauli string, and the weights separately. We will start with encoding the Pauli string and the sign.

Table 3: Boolean variables under the action of conjugating one T gate. Here we omit the sign $(-1)^{r^t}$ for all $\langle G \rangle$ and sign $(-1)^{r^{t+1}}$ for all $\langle TGT^\dagger \rangle$.

$\langle G \rangle$	$x^t z^t r^t$	$\langle TGT^\dagger \rangle$	x^{t+1}	z^{t+1}	r^{t+1}	u
I	$00 r^t$	I	0	z^t	r^t	0
Z	$01 r^t$	Z				
X	$10 r^t$	$\frac{1}{\sqrt{2}}(X+Y)$	1	$\{0,1\}$	r^t	1
Y	$11 r^t$	$\frac{1}{\sqrt{2}}(Y-X)$				

A Pauli string $\mathbf{P} \in \text{PAULI}_n$ can be encoded by $2n$ Boolean variables as 2 bits are needed for each of the n Pauli matrices as $\sigma[x_0, z_0] \otimes \dots \otimes \sigma[x_{n-1}, z_{n-1}]$, where j -th Pauli matrix is indicated by variables x_j and z_j . To encode the sign, only one Boolean variable r is needed. We introduce weighted model counting to interpret the sign by defining $W(r) = -1$ and $W(\bar{r}) = 1$. Thus $P \in \pm\text{PAULI}_n$ can be interpreted as $(-1)^r \otimes_{i \in [n]} \sigma[x_i, z_i]$. For example, consider Boolean formula $r\bar{x}_1 z_1 x_2 z_2$. Its one satisfying assignment is $\{r \rightarrow 1, x_1 \rightarrow 0, z_1 \rightarrow 1, x_2 \rightarrow 1, z_2 \rightarrow 1\} \equiv -Z \otimes Y$. Without loss of generality, we set the initial state to be all zero state $|0\dots 0\rangle$, whose stabilizer group is $\mathcal{S}_{|0\dots 0\rangle} = \{\otimes_{i \in [n]} \mathbf{P}_i \mid \mathbf{P}_i \in \{Z, I\}\} \equiv \{(-1)^r \otimes_{i \in [n]} \sigma[x_i, z_i] \mid x_i = 0, z_i \in \{0, 1\} \text{ and } r = 0\}$. Hence the Boolean formula for the initial state is defined as $F_{\text{init}}(\mathbf{x}^0, \mathbf{z}^0, r) \triangleq \neg r \wedge \bigwedge_{j \in [n]} \neg x_j^0$, where we use superscripts, e.g., r^t, x_1^t, z_1^t , to denote variables at time step t (after t gates from the circuit have been applied). Note that we assign a weight to r only on the final time step, as explained later.

Example 5. Consider the initial state $|00\rangle$ in [Example 4](#). The corresponding constraint at time step 0 is $\neg r^0 \neg x_0^0 \neg x_1^0$, which has satisfying assignments:

$$\left\{ \begin{array}{l} \{r^0 \rightarrow 0, x_0^0 \rightarrow 0, x_1^0 \rightarrow 0, z_0^0 \rightarrow 1, z_1^0 \rightarrow 1\} \\ \{r^0 \rightarrow 0, x_0^0 \rightarrow 0, x_1^0 \rightarrow 0, z_0^0 \rightarrow 1, z_1^0 \rightarrow 0\} \\ \{r^0 \rightarrow 0, x_0^0 \rightarrow 0, x_1^0 \rightarrow 0, z_0^0 \rightarrow 0, z_1^0 \rightarrow 1\} \\ \{r^0 \rightarrow 0, x_0^0 \rightarrow 0, x_1^0 \rightarrow 0, z_0^0 \rightarrow 0, z_1^0 \rightarrow 0\} \end{array} \right\} \equiv \begin{array}{l} \left\{ \begin{array}{l} Z \otimes Z \\ Z \otimes I \\ I \otimes Z \\ I \otimes I \end{array} \right\} \quad \square$$

While we encode those signed Pauli strings using variables from $\{x_j, z_j, r \mid j \in [n]\}$, to encode the weights, we introduce new variables u . When a T_j is performed and $x_j = 1$, which means executing a T gate on j -th qubit with certain stabilizer being either $\pm X$ or $\pm Y$, we set $u = 1$ to indicate a branch of the operator, i.e. $TXT^\dagger = X' = \frac{1}{\sqrt{2}}(X+Y)$ and $TYT^\dagger = Y' = \frac{1}{\sqrt{2}}(Y-X)$. Therefore, for each generalized stabilizer state in a circuit with m gates and n qubits, the encoding uses the set of variables $V^t = \{x_j^t, z_j^t, r^t, u_t \mid j \in [n]\}$, where $t \in \{0, \dots, m\}$ denotes a time step. [Table 3](#) illustrates the details of how the Boolean variables in V^t change over a T gate. Here each satisfying assignment indicates a weighted Pauli string, for example, there are two assignments for a stabilizer $\frac{1}{\sqrt{2}}(X+Y)$.

Using [Table 1](#) and [Table 3](#), given a single-qubit Clifford+T gate \mathbf{G}_j on qubit j at time step t (or $CX_{j,k}$ on qubits j, k), we can derive a Boolean formula

$F_{\mathbf{G}_j}(V^t, V^{t+1})$, abbreviated as \mathbf{G}_j^t , as in the following.

$$\begin{aligned}
 H_j^t &\triangleq r^{t+1} \iff r^t \oplus x_j^t z_j^t \wedge z_j^{t+1} \iff x_j^t \wedge x_j^{t+1} \iff z_j^t \\
 S_j^t &\triangleq r^{t+1} \iff r^t \oplus x_j^t z_j^t \wedge z_j^{t+1} \iff x_j^t \oplus z_j^t \\
 CX_{j,k}^t &\triangleq r^{t+1} \iff r^t \oplus x_j^t z_k^t (x_k^t \oplus \neg z_j^t) \wedge x_k^{t+1} \iff x_k^t \oplus x_j^t \wedge \\
 &\quad z_j^{t+1} \iff z_j^t \oplus z_k^t \\
 T_j^t &\triangleq x_j^{t+1} \iff x_j^t \wedge x_j^t \vee (z_j^{t+1} \iff z_j^t) \wedge \\
 r_i^{t+1} &\iff r^t \oplus x_j^t z_j^t \neg z_j^{t+1} \wedge u_t \iff x_j^t.
 \end{aligned} \tag{3}$$

The above omits additional constraints $v^{t+1} \iff v^t$ for all unconstrained time-step- $t+1$ variables, i.e., for all $v^t \in V_l^t$ with $l \neq j, k$. In fact, it is not necessary to allocate new variables for those unconstrained time-step- $t+1$ variables. The constraint $v^{t+1} \iff v^t$ can be effectively implemented by reusing the Boolean variables v^t for v^{t+1} . Thus for each time step, only a constant number of new variables need to be allocated. For instance, when applying H_j gate, we only need one new variable r_i^{t+1} , since we can reuse the variable of x_j^t for z_j^{t+1} and z_j^t for x_j^{t+1} . And when applying CX_{ij} gate, we need three new variables for r^{t+1} , x_j^{t+1} and z_j^{t+1} . Additionally, since variables for all x_j^0 and z_j^0 with $j \in [n]$ are allocated initially, and as shown in Section 3.4, performing a measurement introduces no new variable, the size of our encoding is $O(n+m)$.

To this end, given a Clifford+ T circuit $C = \mathbf{G}^0 \dots \mathbf{G}^{m-1}$ without measurements, we can build the following Boolean constraint.

$$F_C(V^0, \dots, V^m) \triangleq F_{init}(V^0) \wedge \bigwedge_{t \in [m]} F_{\mathbf{G}^t}(V^t, V^{t+1}). \tag{4}$$

The satisfying assignments of our encoding will represent weighted Pauli strings, so that we can get the density operator at time m by ranging over satisfying assignments $\alpha \in SAT(F_C)$:

$$\rho^m = \sum_{\alpha \in SAT(F_C)} F_C(\alpha) \cdot W(\alpha) \cdot \bigotimes_{j \in [n]} \sigma[\alpha(x_j^m), \alpha(z_j^m)], \tag{5}$$

where $W(r^m) = -1$, $W(\overline{r^m}) = 1$, $W(u_t) = \frac{1}{\sqrt{2}}$, $W(\overline{u_t}) = 1$ for all $t \in \{0, \dots, m\}$ (and all other variables are unbiased). So we will get the weight as $W(\alpha) = W(\alpha(r^m)) \prod_{t \in [m]} W(\alpha(u_t))$. As mentioned before, we only assign weights to r^m where m is the final time step. We allocate a new r^{t+1} for each time step t as we always get r^{t+1} from a constraint related to r^t , but the sign of the final state is given by r^m . So we leave r^t unbiased except when t is the final time step. Additionally, there is no complex number assigned to any weights enabling the application of a classical weighted model counter that allows negative weights. It is worth noting that instead of using satisfying assignments to represent stabilizers in Clifford circuits, we represent weighted Pauli strings as

Table 4: Lookup table for the action of conjugating Pauli gates by rotation gates.

Gate	Matrix Form	In	Out
$RX(\theta)$	$\begin{bmatrix} \cos(\frac{\theta}{2}) & -i\sin(\frac{\theta}{2}) \\ -i\sin(\frac{\theta}{2}) & \cos(\frac{\theta}{2}) \end{bmatrix}$	X Y Z	X $\cos(\theta)Y + \sin(\theta)Z$ $\cos(\theta)Z - \sin(\theta)Y$
$RY(\theta)$	$\begin{bmatrix} \cos(\frac{\theta}{2}) & -\sin(\frac{\theta}{2}) \\ \sin(\frac{\theta}{2}) & \cos(\frac{\theta}{2}) \end{bmatrix}$	X Y Z	$\cos(\theta)Z + \sin(\theta)X$ Y $\cos(\theta)X - \sin(\theta)Z$
$RZ(\theta)$	$\begin{bmatrix} \exp(-i\frac{\theta}{2}) & 0 \\ 0 & \exp(i\frac{\theta}{2}) \end{bmatrix}$	X Y Z	$\cos(\theta)X + \sin(\theta)Y$ $\cos(\theta)Y - \sin(\theta)X$ Z

satisfying assignments, which may be one summand of a stabilizer. For Clifford circuits, there are 2^n satisfying assignments for a n -qubit circuit at each time step. While for Clifford+ T circuits, the satisfying assignments are more than 2^n .

Example 6. Reconsider [Example 4](#), after solving the constraint $F_{init}(V^0) \wedge H_0^0 \wedge CX_{0,1}^1 \wedge T_0^2 \wedge CX_{0,1}^3 \wedge H_0^4$, the satisfying assignments encoding $|\varphi_5\rangle$ will be

$$\left(\begin{array}{l} \{r^5 \rightarrow 0, x_0^5 \rightarrow 0, x_1^5 \rightarrow 0, z_0^5 \rightarrow 1, z_1^5 \rightarrow 0, u_2 \rightarrow 1\}, \\ \{r^5 \rightarrow 1, x_0^5 \rightarrow 1, x_1^5 \rightarrow 0, z_0^5 \rightarrow 1, z_1^5 \rightarrow 0, u_2 \rightarrow 1\}, \\ \{r^5 \rightarrow 0, x_0^5 \rightarrow 0, x_1^5 \rightarrow 0, z_0^5 \rightarrow 0, z_1^5 \rightarrow 1, u_2 \rightarrow 0\}, \\ \{r^5 \rightarrow 0, x_0^5 \rightarrow 0, x_1^5 \rightarrow 0, z_0^5 \rightarrow 1, z_1^5 \rightarrow 1, u_2 \rightarrow 1\}, \\ \{r^5 \rightarrow 1, x_0^5 \rightarrow 1, x_1^5 \rightarrow 0, z_0^5 \rightarrow 1, z_1^5 \rightarrow 1, u_2 \rightarrow 1\}, \\ \{r^5 \rightarrow 0, x_0^5 \rightarrow 0, x_1^5 \rightarrow 0, z_0^5 \rightarrow 0, z_1^5 \rightarrow 0, u_2 \rightarrow 0\} \end{array} \right) \equiv \left(\begin{array}{l} \frac{1}{\sqrt{2}}Z \otimes I \\ -\frac{1}{\sqrt{2}}Y \otimes I \\ I \otimes Z \\ \frac{1}{\sqrt{2}}Z \otimes Z \\ -\frac{1}{\sqrt{2}}Y \otimes Z \\ I \otimes I \end{array} \right)$$

where $w(\bar{r}^5) = 1$, $w(\bar{r}^5) = 1$, $w(u_2) = \frac{\sqrt{2}}{2}$ and $w(\bar{u}_2) = 0$. Here we omit the satisfying assignments for $\{r^t, x_0^t, x_1^t, z_0^t, z_1^t \mid 0 \leq t \leq 4\}$. \square

3.3 Encoding random rotation gates

Our encoding can be extended to other non-Clifford gates, which we demonstrate by adding rotation gates $RX(\theta)$, $RY(\theta)$, and $RZ(\theta)$, where θ is an angle.

In particular, we have $T = \exp(-i\frac{\pi}{8})RZ(\frac{\pi}{4})$, $S = \exp(-i\frac{\pi}{4})RZ(\frac{\pi}{2})$ and $X = -iRX(\pi)$, $Y = -iRY(\pi)$, $Z = -iRZ(\pi)$. Note however that the stabilizer formalism discards the global phase of a state as it updates stabilizers by conjugation, e.g., $TPT^\dagger = (\exp(-i\frac{\pi}{8})RZ(\frac{\pi}{4}))P(\exp(-i\frac{\pi}{8})RZ(\frac{\pi}{4}))^\dagger = RZ(\frac{\pi}{4})PRZ(\frac{\pi}{4})^\dagger$. Based on [Table 4](#), the constraints for rotation gates are as below, where we keep

the coefficients $\cos(\theta)$ and $\sin(\theta)$ by defining the weights of the new variables as $w(u_{1t}) = \cos(\theta)$, $w(\neg u_1) = w(\neg u_2) = 1$ and $w(u_2) = \sin(\theta)$.

$$\begin{aligned}
 RX_j^t &\triangleq z_j^{t+1} \iff z_j^t \wedge z_j^t \vee (x_j^{t+1} \iff x_j^t) \wedge r^{t+1} \iff r^t \oplus z_j^t \neg x_j^t x_j^{t+1} \wedge \\
 &\quad u_{1t} \iff z_j^t (x_j^t x_j^{t+1} \vee \neg x_j^t \neg x_j^{t+1}) \wedge u_{2t} \iff z_j^t (\neg x_j^t x_j^{t+1} \vee x_j^t \neg x_j^{t+1}). \\
 RY_j^t &\triangleq (x_j^t \oplus z_j^t) \iff (x_j^{t+1} \oplus z_j^{t+1}) \wedge (x_j^t \oplus \neg z_j^t) \iff (x_j^t z_j^t \iff x_j^{t+1} \iff z_j^{t+1}) \wedge \\
 &\quad r^{t+1} \iff r^t \oplus z_j^t z_j^{t+1} \wedge u_{1t} \iff (x_j^{t+1} z_j^t \oplus x_j^t z_j^{t+1}) \wedge \\
 &\quad u_{2t} \iff (x_j^{t+1} x_j^t \oplus z_j^{t+1} z_j^t). \\
 RZ_j^t &\triangleq x_j^{t+1} \iff x_j^t \wedge x_j^t \vee (z_j^{t+1} \iff z_j^t) \wedge r^{t+1} \iff r^t \oplus x_j^t z_j^t \neg z_j^{t+1} \wedge \\
 &\quad u_{1t} \iff x_j^t (z_j^t z_j^{t+1} \vee \neg z_j^t \neg z_j^{t+1}) \wedge u_{2t} \iff x_j^t (\neg z_j^t z_j^{t+1} \vee z_j^t \neg z_j^{t+1}).
 \end{aligned}$$

3.4 Measurement

In this section, we consider projective measurement both on a single qubit and on multiple qubits of a quantum system. Single-qubit measurement [42] can be used for extracting only one bit of information from a n -qubits quantum state to effectively protect quantum information [53]. It is also used in random quantum circuits, which contributes to the study of quantum many-body physics [30]. Measurement on multiple qubits is generally used in quantum algorithms, such as in Grover and Shor algorithms, to get the final result. We implement both measurements using *Pauli measurement*, where projectors are Pauli strings.

Single-qubit Pauli Measurement. Let $\mathbb{P}_{k,0} = I \otimes \dots \otimes |0\rangle\langle 0|_k \otimes \dots \otimes I = \frac{1}{2}(Z_k + I^{\otimes n})$ and $\mathbb{P}_{k,1} = I \otimes \dots \otimes |1\rangle\langle 1|_k \otimes \dots \otimes I = \frac{1}{2}(-Z_k + I^{\otimes n})$ for $k \in [n]$. When measuring k -th qubit of a n -qubit state $|\psi\rangle$ using projectors $\{\mathbb{P}_{k,0}, \mathbb{P}_{k,1}\}$, we get two possible outcomes: 0 with probability $p_{k,0}$ and 1 with probability $p_{k,1}$. It follows that $p_{k,0} = \text{Tr}(\mathbb{P}_{k,0} |\psi\rangle\langle\psi|)$, where tr is the trace mapping [48]. As shown in Eq. 2, the density operator $|\psi\rangle\langle\psi|$ can be written using generalized stabilizers i.e., $|\psi\rangle\langle\psi| = \frac{1}{2^n} \sum_{P \in \mathcal{S}_{|\psi\rangle}} P$ for $P = \lambda_P \mathbf{P}$ where $\mathbf{P} \in \text{PAULI}_n$ and $\lambda_P \in \mathbb{R}$. The probability $p_{k,0}$ can be obtained as follows.

$$\begin{aligned}
 p_{k,0} &= \text{tr}(\mathbb{P}_{k,0} |\psi\rangle\langle\psi|) = \text{tr}\left(\frac{1}{2}(I^{\otimes n} + Z_k) |\psi\rangle\langle\psi|\right) \\
 &= \frac{1}{2}(\text{tr}(|\psi\rangle\langle\psi|) + \text{tr}(Z_k |\psi\rangle\langle\psi|)) = \frac{1}{2} + \frac{1}{2^{n+1}} \sum_{\lambda_P \mathbf{P} \in \mathcal{S}_{|\psi\rangle}} \lambda_P \text{tr}(Z_k \mathbf{P})
 \end{aligned} \tag{6}$$

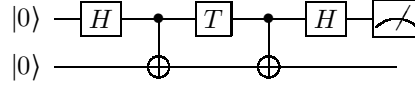
For any $\mathbf{P} \in \text{PAULI}_n$, the trace $\text{tr}(\mathbf{P})$ is non-zero if and only if $\mathbf{P} = I^{\otimes n}$. Given the fact that $\text{tr}(A \otimes B) = \text{tr}(A) \text{tr}(B)$, when considering a n -Pauli string $\mathbf{P} = \mathbf{P}_0 \otimes \dots \otimes \mathbf{P}_{n-1}$, we can express $\text{tr}(\mathbf{P})$ as a product of its constituent Pauli matrices $\text{tr}(\mathbf{P}_0) \dots \text{tr}(\mathbf{P}_{n-1})$. Since it is easy to see that $\text{tr}(X) = \text{tr}(Y) = \text{tr}(Z) = 0$, if there exists a $\mathbf{P}_i \in \{X, Y, Z\}$, then $\text{tr}(\mathbf{P}) = 0$. Furthermore, $\mathbf{P} = Z_k$ if and only if $Z_k \mathbf{P} = I^{\otimes n}$. Thus the result of Eq. 6 can be simplified as $p_k = \frac{1}{2} + \frac{1}{2} \sum_{P=\lambda_P Z_k} \lambda_P$.

In other words, to get the probability of the outcome being 0 on measuring k -th qubit, we need to sum up the weights of all elements Z_k in the flattened Pauli group of Eq. 2. The latter can be encoded as follows, where m is the final time step.

$$F_{M_k}(V^m) \triangleq \bigwedge_{j \in [n]} \neg x_j^m \wedge \bigwedge_{j \in [n], j \neq k} \neg z_j^m \wedge z_k^m \quad (7)$$

A Clifford+ T circuit with a single-qubit Pauli measurement at the end can be encoded by conjoining the constraint of initial state and gates in Eq. 4, and the one for the measurement at the end.

Example 7. Consider the circuit in Example 6 and assume we want to perform single-qubit Pauli measurement on the first qubit using $\{\frac{I \otimes I + Z_0}{2}, \frac{I \otimes I - Z_0}{2}\}$.



By adding the measurement constraint $M_0 \triangleq \bar{x}_0^5 \wedge \bar{x}_1^5 \wedge z_0^5 \wedge \bar{z}_1^5$ to the circuits constraints in Example 6, we get $F_{init}(V^0) \wedge H_0^0 \wedge CX_{0,1}^1 \wedge T_0^2 \wedge CX_{0,1}^3 \wedge H_0^4 \wedge F_{M_0}(V^5)$. The satisfying assignments will be the subset of the solutions in Example 6: $\{\sigma = \{r^5 \rightarrow 0, x_0^5 \rightarrow 0, x_1^5 \rightarrow 0, z_0^5 \rightarrow 1, z_1^5 \rightarrow 0, u_2 \rightarrow 1\}\}$, where we only show the variables in V^5 representing the final state. The resulting probability is $W(\sigma(r^5))W(\sigma(u_2)) = \frac{1}{\sqrt{2}}$. \square

Multi-qubit Pauli Measurement. Similar to the single-qubit Pauli measurement, we can resolve the constraint of multi-qubit Pauli measurement based on the measurement projector \mathbb{P} . Let Q be the set of all qubits and $\bar{Q} \subseteq Q$ be the set of qubits being measured. The projector measuring qubits in \bar{Q} is defined as $\mathbb{P}_{\bar{Q}} = \bigotimes_{q \in \bar{Q}} \mathbb{P}_q$ where $\mathbb{P}_q = (I + Z)/2$ for $q \in \bar{Q}$ and $\mathbb{P}_q = I$ for $q \in Q \setminus \bar{Q}$. We can derive the constraint $F_{\mathbb{P}_q}(x_q^m, z_q^m) = \bar{x}_q^m$ for $q \in \bar{Q}$ and no constraint for $q \in Q \setminus \bar{Q}$. Thus $F_{M_{\bar{Q}}} = \bigwedge_{q \in \bar{Q}} \bar{x}_q^m$. In this way, it is possible to construct the constraint for any computational basis measurement.

We conclude Section 3 with Proposition 2, which also shows that our encoding implements a strong simulation of a universal quantum circuit.

Proposition 2. *Given an n -qubit quantum circuit C , its encoding $F(V^0, \dots, V^m) = F_C(V^0, \dots, V^m) \wedge F_{M_{\bar{Q}}}(V^m)$ with according weight function W and a computational basis projector \mathbb{P} on $q \leq n$ qubits ($q = |\bar{Q}|$), WMC on F computes the probability of measuring the outcome corresponding to \mathbb{P} on circuit C , i.e., we have $\frac{1}{2^q} MC_W(F) = \langle 0 |^{\otimes n} C^\dagger \mathbb{P} C | 0 \rangle^{\otimes n}$.*

4 Experiments

To show the effectiveness of our approach, we implemented a WMC-based simulator in a tool called QCMC. It reads quantum circuits in QASM format [25], en-

codes them to Boolean formulas in conjunctive normal form (CNF) as explained in Section 3, and then uses the weighted model counter GPMC [35] to solve these constraints. We choose GPMC as it is the best solver supporting negative weights in model counting competition 2023 [1]. The resulting implementation and evaluation are publicly available at <https://github.com/System-Verification-Lab/Quokka-Sharp>.

We performed a classical simulation of a quantum circuit comparing our method against two state-of-the-art tools: QuiZX [40] based on ZX-calculus [24] and Quasimodo [60] based on CFLOBDD [61]. In particular, this empirical analysis is performed on two families of circuits: (i) random Clifford+ T circuits, which mimic hard problems arising in quantum chemistry [71] and quantum many-body physics [30]; (ii) random circuits mimicking oracle implementations; (iii) all benchmarks from the public benchmark suite MQT Bench [54], which includes many important quantum algorithms like QAOA, VQE, QNN, Grover, etc. All experiments have been conducted on a 3.5 GHz M2 Machine with MacOS 13 and 16 GB RAM. We set the time limit to be 5 minutes (300 seconds) and include the time to read a QASM file, construct the weighted CNF, and perform the model counting in all reported runtimes.

Results. First, we show the limit of three methods using the set of benchmarks generated by [40]. They construct random circuits with a given number of T gates by exponentiating Pauli unitaries in the form of $\exp(-i(2k+1)\frac{\pi}{4}P)$ where P is a Pauli string and $k \in \{1, 2\}$. We reuse their experimental settings, which gradually increase the T count (through Pauli exponentiation) for $n = 50$ qubits, and we add an experiment with $n = 100$ qubits. Accordingly, we generate 50 circuits with different random seeds for each $n = 50$ and $T \in [0-100]$ and each $n = 100$ and $T \in [0-180]$. We then perform a single-qubit Pauli measurement on the first qubit. We plot the minimal time needed and the rate of successfully getting the answer in 5 minutes among all 50 simulation runs in Figure 1.

Second, we also consider random circuits that more resemble typical oracle implementations — random quantum circuits with varying qubits and depths, which comprise the CX , H , S , and T gates with appearing ratio 10%, 35%, 35%, 20% [52]. The resulting runtimes can be seen in Figure 2.

In addition to random circuits, we empirically evaluated our method on the MQTBench benchmark set [54], measuring all qubits, as is typical in most quantum algorithms. We present a representative subset of results in Table 5. The complete results can be found in Appendix A. All benchmarks are expanded to the Clifford+ T + R gate set, where R denotes $\{RX, RY, RZ\}$. The first two columns list the number of qubits n and the number of gates $|G|$. Columns T and R give the number of T gates and rotation gates. Then, the performance of the weighted model counting tool QCMC, the performance of the ZX-calculus tool QuiZX (ZX), and the performance of CFLOBDD tool Quasimodo (CFLOBDD). The performances are given by the runtime and the corresponding memory usage.

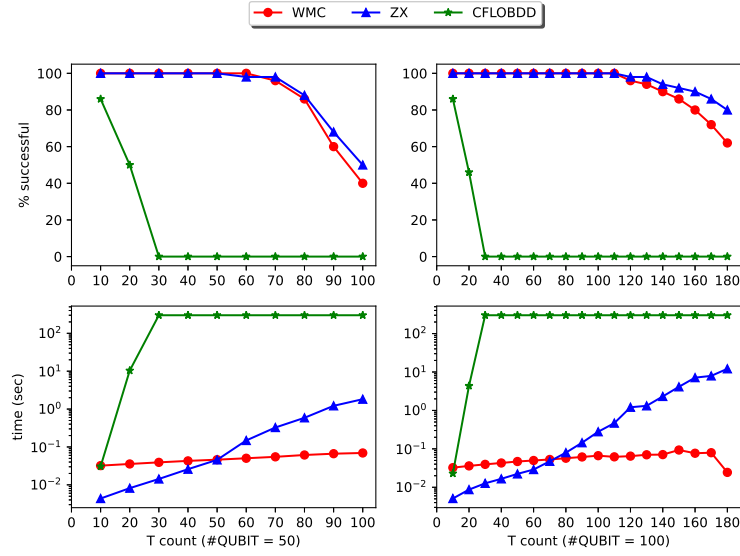
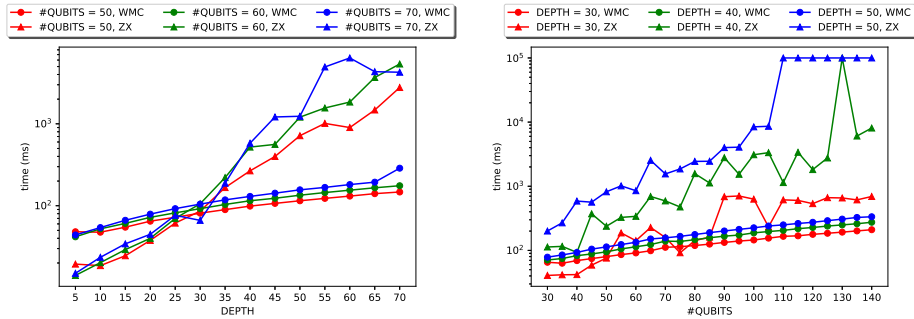


Fig. 1: The upper two figures, both of which have y-axes on a logarithmic scale, are percentages of random 50- and 100-qubit circuits with increasing depth which can be successfully measured in 5 minutes. The below two figures are the minimum running time among the 50 samples for each configuration.



(a) Runtimes for growing qubit counts

(b) Runtimes for growing circuit depth

Fig. 2: Computational basis measurement of typical random Clifford+T circuits. (Both vertical axes are on a logarithmic scale.) CFLOBDD runs out of time for all benchmarks so we do not add it here.

Discussion. For all cases, QuiZX gives algebraic answers while the QCMC and CFLOBDD methods give numerical answers. Because of the imprecision of floating-point arithmetic, we consider a equal to b if $|a - b| < 10^{-8}$. With equality tolerance, all three methods produce the same answers.

Table 5: Results of verifying circuits from MQT bench. For cases within time limit, we give their running time (sec) and corresponding memory usage (MB). We use \times when QuiZX does not support certain benchmarks, while > 300 represents a timeout (5 min). For those benchmarks having a timeout or are not supported, we omit their memory usage by $*$.

Algorithm	n	G	T	R	WMC		ZX		CFLOBDD	
					t(sec)	RSS(MB)	t(sec)	RSS(MB)	t(sec)	RSS(MB)
GHZ State	32	32	0	0	0.044	12.56	0.007	12.28	0.03	354.81
	64	64	0	0	0.049	12.54	0.008	12.30	0.03	356.02
	128	128	0	0	0.048	12.56	0.013	12.44	0.04	355.77
Graph State	16	64	0	0	0.046	12.53	0.005	12.44	0.06	355.68
	32	128	0	0	0.045	12.53	0.008	12.40	0.11	355.39
	64	256	0	0	0.045	12.36	0.015	12.47	243.22	6116.93
Grover's (no ancilla)	4	162	8	58	0.18	12.53	89.18	12.06	0.04	345.56
	5	470	0	195	10.18	12.44	> 300	*	0.07	345.73
	6	1314	0	552	> 300	*	> 300	*	0.21	346.52
QAOA	7	63	0	28	0.03	12.42			0.05	355.98
	9	81	0	36	0.036	12.28	> 300	*	0.05	355.89
	11	99	0	44	0.035	12.41			0.06	355.42
QNN	16	1119	0	400					57.36	2232.14
	32	3775	0	1312	> 300	*	\times	*	> 300	*
	64	13695	0	4672					> 300	*
Quantum Walk (no ancilla)	5	1071	24	448	142.75	12.70			0.13	345.19
	6	2043	24	844	> 300	*	\times	*	0.28	345.58
	7	3975	24	1624	> 300	*			0.80	347.58
QFT	16	520	0	225	0.05	12.34	0.09	12.30	6.58	516.19
	32	2064	0	961	0.11	12.34	0.16	12.53	> 300	*
	64	8224	0	3969	0.37	12.44	0.57	12.32	> 300	*
VQE	14	236	0	82	0.23	12.28			2.84	610.54
	15	253	0	88	0.49	12.14	\times	*	6.29	680.64
	16	270	0	94	0.51	12.50			17.97	943.67
W-state	32	435	0	124	0.11	12.59				
	64	883	0	252	0.28	12.62	\times	*	> 300	*
	128	1779	0	508	0.66	12.63				

For random circuits, Figure 1 illustrates that the minimum runtime barely increases for QCMC, while it seems exponential for QuiZX (note the log scale). However, when the number of qubits is $n = 50$ and the T count is larger than 70, or when, $n = 100$ and the T count is larger than 110, QuiZX has a better success rate, i.e., it completes more simulations than QCMC in 5 minutes. In contrast, CFLOBDD exhibits the lowest success rate among the three methods. When it comes to a typical random Clifford+T circuit Figure 2 shows that the runtime of both QCMC and ZX exhibits a clear correlation with the size of the circuits, while CFLOBDD can not solve all benchmarks in 5 minutes. The proposed implementation consistently outperforms QuiZX by one to three orders of magnitude especially when the size is getting larger (note again the log scale). However, the story changes when considering structural quantum circuits.

For MQT benchmarks, Table 5 shows that QCMC performs better than QuiZX except for GHZ state and Graph State where QCMC is slightly slower in milliseconds. CFLOBDD significantly surpasses QCMC on Grover and quantum walk algorithms, primarily due to the decision diagram-based method’s proficiency in handling circuits featuring large reversible parts and oracles. While for those circuits featuring a large number of rotation gates with various rotation angles, like Graph state, QFT, and VQE, QCMC demonstrates clear advantages. This distinction arises from the fact that when dealing with rotation gates, it might happen that two decision diagram nodes that should be identical in theory, differ by a small margin in practice, obstructing node merging [49]. In contrast, the WMC approach —also numerical in nature— avoids explicit representation of all satisfying assignments, by iteratively computing a sum of products. This not only avoids blowups in space use but, we hypothesize, also avoids numerical instability, a problem that has plagued numerical decision-diagram based approaches [52,49]. In terms of memory usage, CFLOBDD always uses more than 340 MB, in some cases uses more than 6 GB (graph state, $n = 64$), while QCMC and QuiZX use less than 13 MB (OS reported peak resident set size).

Overall, both QCMC and QuiZX outperform CFLOBDD in handling random circuits. Moreover, QCMC has better runtime performance than QuiZX. For structural circuits, QuiZX faces a limitation as it does not efficiently support rotation gates with arbitrary angles, so it is incapable of simulating many quantum algorithms, like VQE, directly. In terms of runtime, CFLOBDD is better at circuits featuring structure, while QCMC performs better at circuits with arbitrary rotation gates. However, CFLOBDD has a significantly higher memory cost compared to both QCMC and QuiZX.

5 Related Work

In this section, we give an overview of the related work on classical simulation of quantum computing with a focus on those methods applying SAT-based solvers.

SAT-based solvers have proven successful in navigating the huge search spaces encountered in various problems in quantum computing [69,45], initial attempts have been made to harness the strengths of satisfiability solvers for the simulation of quantum circuits. For instance, [11] implements a simulator for Clifford circuits based on a SAT encoding (our encoding of H, S, CX in Eq. 3 is similar to theirs). The authors also discuss a SAT encoding for universal quantum circuits, which however requires exponentially large representations, making it impractical. Besides quantum circuits, [10] presents symQV, a framework for verifying quantum programs in a quantum circuit model, which allows to encode the verification problem in an SMT formula, which can then be checked with a δ -complete decision process. There is an SMT theory for quantum computing [22].

Another method is based on decision diagrams (DDs) [2,16], which represent many Boolean functions succinctly, while allowing manipulation operations with-

out decompression. DD methods for pseudo-Boolean functions include Algebraic DDs (ADD) [9,23,66] and various “edge-valued” ADDs [43,63,70,57]. The application of DDs to quantum circuit simulation, by viewing a quantum state as a pseudo-Boolean function, was pioneered with QuiDDs [67] and further developed with Quantum Multi-valued DDs [46], Tensor DDs [37] and CFLOBDDs [61]. All but CFLOBDD are essentially ADDs with complex numbers.

Another way is to translate quantum circuits into ZX-diagrams [24], which is a graphical calculus for quantum circuits equipped with powerful rewrite rules.

Classical simulation is commonly used for the verification of quantum circuits, with extensive research focused on their equivalence checking [68,7,5]. It can also be applied to bug hunting in quantum circuits. In [21], the authors proposed a tree automata to compactly represent quantum states and gates algebraically, framing the verification problem as a Hoare triple.

6 Conclusions

In this work, we propose a generalized stabilizer formalism formulated in terms of a stabilizer group. Based on this, we provide an encoding for various universal gate sets as a weighted model counting problem with only negative weights, obviating the need for complex numbers that are not supported by existing WMC tools. Besides T gates, we also extend our encoding to general rotation gates. Furthermore, we demonstrate how to perform computational basis measurements using this encoding, enabling strong quantum circuit simulation.

We have implemented our method in an open source tool QCMC. To give empirical results on the practicality of our method, we applied it to a variety of benchmarks comparing one based on ZX-calculus and one based on decision diagrams. Experimental results show that our approach outperforms it in most cases, particularly with circuits of large sizes. The performance of our approach is quite different from the other approaches, demonstrating the unique potential of WMC in various use cases. It will be interesting to see whether WMC tools can improve up on this should these new benchmarks be included in the WMC competition.

This work provides a new benchmark paradigm for weighted model counting problems. In the future, it will be interesting to apply our encoding to approximate weighted model counting [19,28]. Moreover, using weighted samplers [44,33], we could realize weak circuit simulation using the same encoding. The main obstacle now is to allow negative weights in approximate weighted model counters and samplers. Additionally, it will also be interesting to explore more applications of this encoding, such as checking the equivalence of two quantum circuits and entanglement purification.

References

1. Model counting competition 2023. <https://mccompetition.org/>. Accessed: 2024-01-07.
2. Akers. Binary decision diagrams. *IEEE Transactions on Computers*, C-27(6):509–516, 1978.
3. Matthew Amy, Owen Bennett-Gibbs, and Neil J. Ross. Symbolic synthesis of Clifford circuits and beyond. *Electronic Proceedings in Theoretical Computer Science*, 394:343–362, November 2023.
4. Simon Anders and Hans J. Briegel. Fast simulation of stabilizer circuits using a graph-state representation. *Physical Review A*, 73(2), February 2006.
5. Ebrahim Ardeshir-Larijani, Simon J. Gay, and Rajagopal Nagarajan. Equivalence checking of quantum protocols. In Nir Piterman and Scott A. Smolka, editors, *Tools and Algorithms for the Construction and Analysis of Systems*, pages 478–492, Berlin, Heidelberg, 2013. Springer Berlin Heidelberg.
6. Ebrahim Ardeshir-Larijani, Simon J. Gay, and Rajagopal Nagarajan. Verification of concurrent quantum protocols by equivalence checking. In *TACAS*, pages 500–514. Springer, 2014.
7. Ebrahim Ardeshir-Larijani, Simon J. Gay, and Rajagopal Nagarajan. Verification of concurrent quantum protocols by equivalence checking. In Erika Ábrahám and Klaus Havelund, editors, *Tools and Algorithms for the Construction and Analysis of Systems*, pages 500–514, Berlin, Heidelberg, 2014. Springer Berlin Heidelberg.
8. Frank Arute et al. Quantum supremacy using a programmable superconducting processor. *Nature*, 574:505–510, 2019.
9. R. I. Bahar, E. A. Frohm, C. M. Gaona, G. D. Hachtel, E. Macii, A. Pardo, and F. Somenzi. Algebraic decision diagrams and their applications. In *Proceedings of 1993 International Conference on Computer Aided Design (ICCAD)*, pages 188–191, 1993.
10. Fabian Bauer-Marquart, Stefan Leue, and Christian Schilling. symQV: Automated symbolic verification of quantum programs. In Marsha Chechik, Joost-Pieter Katoen, and Martin Leucker, editors, *Formal Methods*, pages 181–198, Cham, 2023. Springer International Publishing.
11. Lucas Berent, Lukas Burgholzer, and Robert Wille. Towards a SAT encoding for quantum circuits: A journey from classical circuits to clifford circuits and beyond. Schloss Dagstuhl - Leibniz-Zentrum für Informatik, 2022.
12. Armin Biere, Marijn Heule, Hans van Maaren, and Toby Walsh, editors. *Handbook of Satisfiability*, volume 185 of *Frontiers in Artificial Intelligence and Applications*. IOS Press, 2009.
13. Sebastiaan Brand, Tim Coopmans, and Alfons Laarman. Quantum graph-state synthesis with SAT. In *Proceedings of the 14th International Workshop on Pragmatics of SAT co-located with the 26th International Conference on Theory and Applications of Satisfiability Testing (SAT 2023), Alghero, Italy, July 4, 2023*, volume 3545 of *CEUR Workshop Proceedings*, pages 1–13. CEUR-WS.org, 2023.
14. Sergey Bravyi and David Gosset. Improved classical simulation of quantum circuits dominated by Clifford gates. *Phys. Rev. Lett.*, 116:250501, Jun 2016.
15. Sergey Bravyi, Ruslan Shaydulin, Shaohan Hu, and Dmitri Maslov. Clifford circuit optimization with templates and symbolic Pauli gates. *Quantum*, 5:580, November 2021.
16. Randal E. Bryant. Graph-based algorithms for Boolean function manipulation. *IEEE Trans. Computers*, 35(8):677–691, 1986.

17. Lukas Burgholzer and Robert Wille. Improved DD-based equivalence checking of quantum circuits. In *2020 25th Asia and South Pacific Design Automation Conference (ASP-DAC)*, pages 127–132. IEEE, 2020.
18. A. R. Calderbank and Peter W. Shor. Good quantum error-correcting codes exist. *Phys. Rev. A*, 54:1098–1105, Aug 1996.
19. Supratik Chakraborty, Daniel Fremont, Kuldeep Meel, Sanjit Seshia, and Moshe Vardi. Distribution-aware sampling and weighted model counting for sat. In *Proceedings of the AAAI Conference on Artificial Intelligence*, volume 28, 2014.
20. Mark Chavira and Adnan Darwiche. On probabilistic inference by weighted model counting. *Artificial Intelligence*, 172(6):772–799, 2008.
21. Yu-Fang Chen, Kai-Min Chung, Ondřej Lengál, Jyun-Ao Lin, Wei-Lun Tsai, and Di-De Yen. An automata-based framework for verification and bug hunting in quantum circuits. *Proc. ACM Program. Lang.*, 7(PLDI), jun 2023.
22. Yu-Fang Chen, Philipp Rümmer, and Wei-Lun Tsai. A theory of cartesian arrays (with applications in quantum circuit verification). In *International Conference on Automated Deduction*, pages 170–189. Springer, 2023.
23. Edmund M Clarke, Kenneth L McMillan, Xudong Zhao, Masahiro Fujita, and Jerry Yang. Spectral transforms for large boolean functions with applications to technology mapping. In *Proceedings of the 30th international Design Automation Conference*, pages 54–60, 1993.
24. Bob Coecke and Ross Duncan. Interacting quantum observables: categorical algebra and diagrammatics. *New Journal of Physics*, 13(4):043016, 2011.
25. Andrew Cross, Ali Javadi-Abhari, Thomas Alexander, Niel De Beaudrap, Lev S. Bishop, Steven Heidel, Colm A. Ryan, Prasahnt Sivarajah, John Smolin, Jay M. Gambetta, and Blake R. Johnson. OpenQASM3: A broader and deeper quantum assembly language. *ACM Transactions on Quantum Computing*, 3(3):1–50, September 2022.
26. Christopher M. Dawson and Michael A. Nielsen. The Solovay-Kitaev algorithm. *Quantum Inf. Comput.*, 6(1):81–95, 2006.
27. M. Van den Nest. Classical simulation of quantum computation, the Gottesman-Knill theorem, and slightly beyond. *Quantum Information & Computation*, 10(3):258–271, 2010.
28. Stefano Ermon, Carla P Gomes, Ashish Sabharwal, and Bart Selman. Embed and project: Discrete sampling with universal hashing. *Advances in Neural Information Processing Systems*, 26, 2013.
29. Nick Feng, Lina Marsso, Mehrdad Sabetzadeh, and Marsha Chechik. Early verification of legal compliance via bounded satisfiability checking. In Constantin Enea and Akash Lal, editors, *Computer Aided Verification*, pages 374–396, Cham, 2023. Springer Nature Switzerland.
30. Matthew P.A. Fisher, Vedika Khemani, Adam Nahum, and Sagar Vijay. Random quantum circuits. *Annual Review of Condensed Matter Physics*, 14(1):335–379, March 2023.
31. Héctor J García, Igor L Markov, and Andrew W Cross. On the geometry of stabilizer states. *Quantum Information & Computation*, 14(7&8):683–720, 2014.
32. Simon J. Gay. Stabilizer states as a basis for density matrices. *CoRR*, abs/1112.2156, 2011.
33. Priyanka Golia, Mate Soos, Sourav Chakraborty, and Kuldeep S Meel. Designing samplers is easy: The boon of testers. In *2021 Formal Methods in Computer Aided Design (FMCAD)*, pages 222–230. IEEE, 2021.
34. Daniel Gottesman. *Stabilizer codes and quantum error correction*. PhD thesis, California Institute of Technology, 1997.

35. Kenji Hashimoto. GPMC. <https://git.trs.css.i.nagoya-u.ac.jp/k-hasimt/GPMC>, 2020.
36. Xin Hong, Yuan Feng, Sanjiang Li, and Mingsheng Ying. Equivalence checking of dynamic quantum circuits. In *Proceedings of the 41st IEEE/ACM International Conference on Computer-Aided Design, ICCAD '22*, New York, NY, USA, 2022. Association for Computing Machinery.
37. Xin Hong, Xiangzhen Zhou, Sanjiang Li, Yuan Feng, and Mingsheng Ying. A tensor network based decision diagram for representation of quantum circuits. *ACM Trans. Design Autom. Electr. Syst.*, 27(6):60:1–60:30, 2022.
38. Cupjin Huang, Fang Zhang, Michael Newman, Junjie Cai, Xun Gao, Zhengxiong Tian, Junyin Wu, Haihong Xu, Huanjun Yu, Bo Yuan, Mario Szegedy, Yaoyun Shi, and Jianxin Chen. Classical simulation of quantum supremacy circuits, 2020.
39. Richard Jozsa and Maarten Van den Nest. Classical simulation complexity of extended Clifford circuits. *Quantum Inf. Comput.*, 14(7-8):633–648, 2014.
40. Aleks Kissinger and John van de Wetering. Simulating quantum circuits with ZX-calculus reduced stabiliser decompositions. *Quantum Science and Technology*, 7(4):044001, July 2022.
41. Vadym Kliuchnikov. Synthesis of unitaries with Clifford+T circuits. *arXiv e-prints*, page arXiv:1306.3200, June 2013.
42. Lucas Kocia and Mohan Sarovar. Classical simulation of quantum circuits using fewer gaussian eliminations. *Phys. Rev. A*, 103:022603, Feb 2021.
43. Y-T Lai, Massoud Pedram, and Sarma BK Vrudhula. EVBDD-based algorithms for integer linear programming, spectral transformation, and function decomposition. *IEEE Transactions on Computer-Aided Design of Integrated Circuits and Systems*, 13(8):959–975, 1994.
44. Kuldeep S Meel, Suwei Yang, and Victor Liang. Inc: A scalable incremental weighted sampler. In *FMCAD 2022*, volume 3, page 205. TU Wien Academic Press, 2022.
45. Giulia Meuli, Mathias Soeken, and Giovanni De Micheli. SAT-based {CNOT, T} quantum circuit synthesis. In Jarkko Kari and Irek Ulidowski, editors, *Reversible Computation*, pages 175–188, Cham, 2018. Springer International Publishing.
46. D Michael Miller and Mitchell A Thornton. QMDD: A decision diagram structure for reversible and quantum circuits. In *36th International Symposium on Multiple-Valued Logic (ISMVL'06)*, pages 30–30. IEEE, 2006.
47. Yunseong Nam, Yuan Su, and Dmitri Maslov. Approximate quantum fourier transform with $o(n \log(n))$ t gates. *npj Quantum Information*, 6(1):26, 2020.
48. Michael A Nielsen and Isaac L Chuang. Quantum information and quantum computation. *Cambridge: Cambridge University Press*, 2(8):23, 2000.
49. Philipp Niemann, Alwin Zulehner, Rolf Drechsler, and Robert Wille. Overcoming the tradeoff between accuracy and compactness in decision diagrams for quantum computation. *IEEE Transactions on Computer-Aided Design of Integrated Circuits and Systems*, 39(12):4657–4668, 2020.
50. Umut Oztok and Adnan Darwiche. A top-down compiler for sentential decision diagrams. *IJCAI'15*, page 3141–3148. AAAI Press, 2015.
51. Hakop Pashayan, Stephen D. Bartlett, and David Gross. From estimation of quantum probabilities to simulation of quantum circuits. *Quantum*, 4:223, January 2020.
52. Tom Peham, Lukas Burgholzer, and Robert Wille. Equivalence checking of quantum circuits with the ZX-calculus. *IEEE Journal on Emerging and Selected Topics in Circuits and Systems*, 12(3):662–675, September 2022.

53. Stefano Polla, Gian-Luca R. Anselmetti, and Thomas E. O'Brien. Optimizing the information extracted by a single qubit measurement. *Phys. Rev. A*, 108:012403, Jul 2023.
54. Nils Quetschlich, Lukas Burgholzer, and Robert Wille. Mqt bench: Benchmarking software and design automation tools for quantum computing. *Quantum*, 7:1062, July 2023.
55. Robert Raussendorf and Hans J. Briegel. A one-way quantum computer. *Phys. Rev. Lett.*, 86:5188–5191, May 2001.
56. Tian Sang, Fahiem Bacchus, Paul Beame, Henry A. Kautz, and Toniann Pitassi. Combining component caching and clause learning for effective model counting. In *International Conference on Theory and Applications of Satisfiability Testing*, 2004.
57. Scott Sanner and David McAllester. Affine algebraic decision diagrams (AADDs) and their application to structured probabilistic inference. In *Proceedings of the 19th International Joint Conference on Artificial Intelligence, IJCAI'05*, pages 1384–1390, San Francisco, CA, USA, 2005. Morgan Kaufmann Publishers Inc.
58. Sarah Schneider, Lukas Burgholzer, and Robert Wille. A SAT encoding for optimal Clifford circuit synthesis. In *Proceedings of the 28th Asia and South Pacific Design Automation Conference, ASPDAC '23*. ACM, January 2023.
59. Irfansha Shaik and Jaco van de Pol. Optimal layout synthesis for quantum circuits as classical planning. *arXiv preprint arXiv:2304.12014*, 2023.
60. Meghana Sistla, Swarat Chaudhuri, and Thomas Reps. Symbolic quantum simulation with quasimodo. In Constantin Enea and Akash Lal, editors, *Computer Aided Verification*, pages 213–225. Springer, 2023.
61. Meghana Sistla, Swarat Chaudhuri, and Thomas Reps. Weighted context-free-language ordered binary decision diagrams. *arXiv preprint arXiv:2305.13610*, 2023.
62. A. M. Steane. Error correcting codes in quantum theory. *Phys. Rev. Lett.*, 77:793–797, Jul 1996.
63. Paul Tafertshofer and Massoud Pedram. Factored edge-valued binary decision diagrams. *Formal Methods in System Design*, 10(2):243–270, 1997.
64. Dimitrios Thanos, Tim Coopmans, and Alfons Laarman. Fast equivalence checking of quantum circuits of Clifford gates. In Étienne André and Jun Sun, editors, *Automated Technology for Verification and Analysis*, pages 199–216, Cham, 2023. Springer Nature Switzerland.
65. Géza Tóth and Otfried Gühne. Entanglement detection in the stabilizer formalism. *Phys. Rev. A*, 72:022340, Aug 2005.
66. George F Viamontes, Igor L Markov, and John P Hayes. Improving gate-level simulation of quantum circuits. *Quantum Information Processing*, 2(5):347–380, 2003.
67. G.F. Viamontes, I.L. Markov, and J.P. Hayes. High-performance QuIDD-based simulation of quantum circuits. In *Proceedings Design, Automation and Test in Europe Conference and Exhibition*, volume 2, pages 1354–1355 Vol.2, 2004.
68. Qisheng Wang, Riling Li, and Mingsheng Ying. Equivalence checking of sequential quantum circuits. *IEEE Transactions on Computer-Aided Design of Integrated Circuits and Systems*, 41(9):3143–3156, 2022.
69. Robert Wille, Hongyan Zhang, and Rolf Drechsler. ATPG for reversible circuits using simulation, Boolean satisfiability, and pseudo Boolean optimization. In *2011 IEEE Computer Society Annual Symposium on VLSI*, pages 120–125, 2011.
70. Nic Wilson. Decision diagrams for the computation of semiring valuations. In *Proceedings of the 19th international joint conference on Artificial intelligence*, pages 331–336, 2005.

71. Jerimiah Wright, Meenambika Gowrishankar, Daniel Claudino, Phillip C. Lotshaw, Thien Nguyen, Alexander J. McCaskey, and Travis S. Humble. Numerical simulations of noisy quantum circuits for computational chemistry. *Materials Theory*, 6(1):18, 2022.
72. Yihong Zhang, Yifan Tang, You Zhou, and Xiongfeng Ma. Efficient entanglement generation and detection of generalized stabilizer states. *Phys. Rev. A*, 103:052426, May 2021.
73. Alwin Zulehner and Robert Wille. One-pass design of reversible circuits: Combining embedding and synthesis for reversible logic. *IEEE Transactions on Computer-Aided Design of Integrated Circuits and Systems*, 37(5):996–1008, 2018.

A Appendix

Here we show the results of remaining benchmarks in MQT bench, where [Table 6](#) and [Table 7](#) shows results of simulating measurements on scalable benchmarks and non-scalable benchmarks respectively [54].

Table 6: Results of verifying scalable Benchmarks in MQTbench.

Algorithm	n	G	T	R	WMC		ZX		CFLOBDD	
					t(sec)	RSS(MB)	t(sec)	RSS(MB)	t(sec)	RSS(MB)
Amplitude Estimation	16	725	0	390	> 300	*	> 300	*	> 300	*
	32	2485	0	1297						
	64	9077	0	4642						
	128	34549	0	17467						
Deutsch Jozsa	16	160	0	56	0.05	12.56	0.008	12.45	0.04	355.92
	32	470	0	195	0.05	12.59	0.012	12.69	0.04	355.43
	64	1314	0	552	0.07	12.55	0.022	12.44	0.07	355.54
	128	3319	0	1344	0.1	12.67	0.04	12.47	0.1	356.05
Grover's (v-chain)	5	458	24	165	23.41	12.75	0.05	12.43	0.07	355.91
	7	1058	48	388	> 300	*	0.28	12.53	0.11	355.72
	9	1314	0	552	> 300	*	1.19	12.48	0.32	365.06
	11	3319	0	1344	> 300	*	4.86	12.43	1.10	386.73
Portfolio Optimization with QAOA	7	315	0	161	41.17	12.64			0.12	355.64
	9	470	0	195	> 300	*	×	*	0.32	360.84
	11	1314	0	552	> 300	*			1.20	370.64
Portfolio Optimization with VQE	4	134	8	32	0.09	12.58			0.062	355.53
	8	412	0	64	19.83	12.58	×	*	0.17	356.44
	16	1400	0	128	> 300	*			84.2	1069.14
QPE exact	16	1119	0	400					5.39	638.031
	32	3775	0	1312	> 300	*	×	*	> 300	*
	64	13695	0	4672					> 300	*
QPE inexact	16	532	0	225					5.61	635.56
	32	3775	0	1312	> 300	*	×	*	> 300	*
	64	13695	0	4672					> 300	*
Quantum Walk (v-chain)	5	325	72	64	6.88	12.58	0.038	12.45	0.04	355.43
	11	1585	360	344	> 300	*	0.14	12.48	0.26	355.73
	17	3975	24	1624	> 300	*	0.30	12.45	0.26	367.69
Real Amplitudes ansatz with Random Parameters	16	680	0	128						
	32	2128	0	256	> 300	*	> 300	*	> 300	*
	64	7328	0	512						
	128	26944	0	1024						
Efficient SU2 ansatz with Random Parameters	16	680	0	289					53.58	1114.42
	32	2128	0	576	> 300	*	> 300	*	> 300	*
	64	7328	0	1141					> 300	*
Two Local ansatz with Random Parameters	16	680	0	128					42.61	1120.14
	32	2128	0	256	> 300	*	×	*	> 300	*
	64	7328	0	512					> 300	*
	128	26944	0	1024					> 300	*

Table 7: Results of verifying non-scalable Benchmarks in MQTbench.

Algorithm	n	G	T	R	WMC		ZX		CFLOBDD	
					time(sec)	RSS(MB)	time(sec)	RSS(MB)	time(sec)	RSS(MB)
Ground State	4	120	0	48	0.075	12.58			0.05	355.89
	12	648	0	144	> 300	*	×	*	1.99	393.02
	14	840	0	168	> 300	*			10.60	674.30
Pricing Call	7	339	48	127					0.06	355.95
	11	727	96	255	> 300	*	×	*	0.11	355.48
	15	1547	144	527					0.32	362.28
	19	4101	192	1375					2.36	386.5
Pricing Put	7	341	48	127					0.06	355.95
	11	733	96	255	> 300	*	×	*	0.11	355.55
	15	1565	144	527					0.32	360.30
	19	4119	192	1375					2.38	387.09
Routing	2	43	0	16	0.05	12.55			0.03	346.30
	6	135	96	48	0.34	12.39	×	*	0.05	344.56
	12	135	96	48	60.51	12.63			1.40	368.39
Shor	18	29935	128	11281	> 300	*	> 300	*	> 300	*
	18	29935	128	11185						
Travelling Salesman	4	165	0	48	0.13	12.55			0.04	354.64
	9	390	0	108	2.77	12.59	×	*	0.2	362.59
	16	705	0	192	20.18	12.61			27.73	687.38